行政院國家科學委員會專題研究計畫成果報告

三 維 跌 流 平 台 渠 道 流 場 之 流 動 不 穩 定 分 析
Flow Instability in the 3-D Backward-Facing Step Channels

計畫編號：NSC89-2212-E-002-141

執行期限：89 年 8 月 1 日至 90 年 7 月 31 日

主持人：蔣 德 普 國立台灣大學造船及海洋工程學系 教授

Abstract

A numerical investigation of laminar flow over a backward-facing step is presented within the transient context. The analysis is concerned with the step geometry and flow conditions reported by Armaly et al.[1]. The present transient analysis increases our understanding of the complex interaction of the end-wall-induced vortices and the mainstream flow. This helps to reveal the mechanism responsible for the increasing penetration of the three-dimensional flow structure into a region near the midplane of the channel, at which the flow is essentially two-dimensional.

中文摘要

本文以有限容積數值方法模擬三維跌流渠道流場(Armaly et al.[1] 實驗)，探討側壁效應於整個流場發展之時變性歷程。在啟始時間裡，流場的變化係以幾何形狀(即跌流平台)為主控，渠道中央應維持著二維屬性。當跌流平台主控的流場已達完全發展階段，側壁影響漸趨顯著，其將調整主流原屬二維屬性但較弱的流場結構，此即所謂有限渠寬下側壁面之三維效應。

1. Introduction

Flow separation has a considerable impact on the flow structure and has been the subject of intensive study for many years. Owing to the geometrical simplexity and the availability of experimental data[1], there is considerable incentive to study the flow in a sudden expansion channel. Experimental investigations into the backward-facing step problem by Armaly et al.[1] have shed light on some major flow features. An attempt to increase our understanding of the process by which the flow proceeds to time-dependency has prompted researchers to resort to numerical simulation of this problem. Much previous effort has focused on two-dimensional study due to insufficient computer power. It is only in the last few years that significant progress has been made and analyses based on the computational fluid dynamics technique developed to the point where three-dimensional calculations have become feasible and affordable for many research institutes[2-4]. The present study is a continuation of our previous investigation into steady flows over a backward-facing step[5-6]. Our attention has focused on transient issues that have been much less explored.

2. Working equations and discretization method

Investigation into the unsteady nature of a flow requires the solution of a set of nonlinear partial differential equations that express mass and momentum conservation. For incompressible flow, the continuity equation must not only preserve mass conservation but also enforce a constraint on the velocity field. Thus, the pressure in the following primitive-variable equations has an implicit

$$\frac{\partial u_n}{\partial t}+\frac{\partial}{\partial x_m}(u_m u_n)=-\frac{\partial p}{\partial x_n}+\frac{1}{Re*}\frac{\partial^2 x_n}{\partial x_m \partial x_m} \quad (1)$$

$$\frac{\partial u_m}{\partial x_m}=0 \quad (2)$$

In the above elliptic-parabolic mixed type differential equations, we normalize all variables to make future application an easier task. In the normalization, we chose the mean velocity at the inlet plane $U_{mean}(\equiv 1)$ and ρU_{mean}^2 as the reference quantities for the working variables $\underline{u}$ and p, respectively. The independent variables $\underline{x}$ and t are made dimensionless by the upstream channel height $h(\equiv 1)$ and h/U_{mean}, respectively. This leads to the Reynolds number $Re^* (\equiv \frac{\rho U_{mean} h}{\mu})$ shown in equation (1). The Reynolds number definition involves the fluid viscosity, μ, and the fluid density, ρ. It is worth noting that the definition of the Reynolds number Re^* differs from $Re (\equiv \frac{\rho U_{mean}(2h)}{\mu})$ used by Armaly et al.[1]. This implies that $Re = 2Re^*$. For comparison purposes, throughout this paper, we adopt the notation of Armaly et al.[1] for the Reynolds number Re.

Working equations (1-2) are integrated in their respective finite volume, each of which are associated with a particular primitive variable and is placed on the centroid of the finite volume. A serious problem, which has been encountered when simulating incompressible Navier-Stokes equations, is checkerboard pressure oscillations. To overcome this difficulty, field variables are stored at staggered grids. Numerical simulation of incompressible Navier-Stokes equations entails another instability, which is evident from the oscillatory velocities, when dominated advective terms are discretized using centered schemes. The loss of convective stability is particularly pronounced in multi-dimensional flow simulations. To fix this problem, we have modified the QUICK scheme of Leonard[7] and implemented it in non-uniform grids to resolve this instability problem and avoid the false diffusion error. Discretization of other derivatives is performed using the centered- scheme for revealing their elliptic characters.

In solving the finite volume discretized equations for (1-2), we abandon the coupled approach due to the need for much more disk storage space compared to the space needed when solving these equations separately by the SIMPLE-C solution algorithm (Van Doormaal and Raithby[8]). Use of this algorithm has been found to produce accurate results with a good rate of convergence. The pressure field is solved using the pressure correction method. In the staggered meshes, there are no storage points for the pressure at the domain boundary. Specification of pressure boundary conditions is not needed. In this study, the Euler implicit method is employed to approximate the time derivative term.

3. Problem description and boundary condition

The channel, as configured in Fig. 1, is characterized as having a backward-facing step, across which a three-dimensional channel flow develops into a wider channel with an expansion ratio of H/h = 1.9423. Analyses were considered under conditions reported by Armaly et al.[1]. Direct comparisons with the physical experiments have thus been made to achieve the validation of the numerical results. Using the step geometry S = 0.9423 and the flow conditions of Armaly et al.[1], our analysis was carried out on the basis of the Reynolds numbers Re = 100, 389, and 1000.

Throughout our analysis, inlets of the physical domain were mainly chosen at the step plane. We prescribe at the step plane a fully developed velocity profile given by

$$\underline{u} = (u, v, w) = (\frac{48}{\alpha \pi^3} \beta(y, z), 0, 0), \tag{3}$$

$$\alpha = 1 - [\frac{192B}{\pi^5} (\sum_{i=1,3,5,...}^{300} \frac{\tanh(\xi)}{i^5})], \tag{4}$$

$$\beta = \sum_{i=1,3,5,...}^{300} -1^{\frac{i-1}{2}} (1 - \frac{\cosh(2z\xi - \xi)}{\cosh(\xi)}) \frac{\cos(2y\xi)}{i^3}, \tag{5}$$

$$\xi(i) = (\frac{\pi}{2B}) i \tag{6}$$

In equations (4) and (6), B is known as the span of the channel. In the channel far enough downstream of the step plane, the flow will again be parabolic.

For practical reasons, it is desirable to truncate the analysis domain downstream of the step plane with a distance of $50h$. Truncating the analysis at the synthetic outlet is desirable; otherwise, computer time and storage requirements will greatly exceed the limits of today's computers. Thanks to the experimental confirmation of the flow symmetry about $y = 0$[1], it is only necessary to seek a solution in a half channel ($y \geq 0$). The symmetric boundary condition is prescribed on the midplane of the channel. On the rest of boundaries, where the no-slip wall assumption holds, we prescribe zero velocities on the roof, floor, step plane, and the vertical end wall.

4. Results and discussion

Before moving on to a discussion of the transient results, it is appropriate to justify our steady-state calculations. Figure 2 plots the results of streamwise velocity profiles at the symmetry plane for Re = 100, 389, and 1000. Figures 2 shows that there is generally good agreement between the present results and experimental data of Armaly et al.[1] and excellent agreement with two-dimensional numerical results for Re = 100 and 389. It can be inferred from these results that the channel width $B = 35h$ is sufficiently wide to ignore the end wall boundary layer effect on the channel flow in the immediate vicinity of the midplane, $y = 0$, for Reynolds numbers less that 400. This is not the case as Re was increased further up to a value of approximately 1000. For the case of Re = 1000, disagreement is pronounced in the range of $10h \leq x \leq 25h$. We find that the worst agreement is where the roof eddy (2-D case) shows its presence. This raises the question of how the roof eddy can alter the flow through a channel expansion. It is our objective to determine whether the vertical end wall will affect the flow development into the wider straight channel.

To gain a better understanding of this phenomenon, we conducted a transient simulation of the backward facing problem for Re = 1000. In this study, we adopted Grid-C in our three-dimensional steady flow analysis and a coarser grid, namely Grid-D, in the transient analysis. For details of the grid sizes and time increments used in this study, see Table 1. The time-evolution of the streamwise velocity profiles and the time history of x_1, x_4, and x_5 are plotted on the symmetry-plane $y = 0$, in Fig. 3 and Fig. 4 respectively. It can be concluded from Figs. 3 and 4 that at a time $t < 100$, the flow development in the channel is primarily attributable to the step geometry. The shear stresses exerted on the end-wall are too weak to lead to a strong three-dimensional flow. In our three-dimensional transient analysis the streamwise velocity profiles at the plane of symmetry are not appreciably different from those of the two-dimensional results for Re = 1000 at a time $t < 100$ (Fig. 3). This observation is consistent with the x_1, x_4, and x_5 plots against time (Fig. 4). At $t <$ 100, the lengths of separation and reattachment do not differ between the two- and three-dimensional analyses. When the time reaches t = 100, the primary reattachment length starts to differ for the two analyses. The difference in the x_1 value sheds light on the influence of the end-wall on the subsequent flow development. As Figs. 3 shows, the three-dimensional streamwise velocity profiles on the symmetry plane no longer follow the two-dimensional profiles. This implies that at a time subsequent to t = 100, the end-wall effect has an increasingly important effect on the vortical flow development into the expansion channel. One can clearly see from Fig. 4 a marked change in the time histories of x_1, x_4, and x_5. This explains why the two-dimensional nature of the flow evolves in the expansion flow development. Revealed by Fig. 4 is the disappearance of the roof eddy on the channel midplane at a time, which is approximately equal to 700. Subsequent to t = 1000, the flow gradually reaches the periodically steady state in the sense that the oscillating amplitude of the primary reattachment length, x_1, takes on 1/1000 of its mean velocity. The time periodicity is around 200 (Fig. 4). Such a fluctuation has a tendency to decay as t

keeps increasing and, finally, the flow approaches a truly steady state.

Given that flow separation is of fundamental importance in many processing industries, it is instructive to identify its presence. This is followed by a rigorous determination of its extension into the channel of the present interest. Our desire to depict the separation bubble prompted us to adopt the theoretically rigorous theory of topology, we plot limiting streamlines on the channel roof and floor in Figs. 5 and 6. At the very beginning of the flow evolution, the secondary bubble does appear on the roof of the channel. This roof eddy is situated in between the lines of separation and reattachment. These initially parallel critical lines are found to extend all the way to the midplane (Fig. 5(a)). This suggests that the end-wall effect exists only in the limited range near the end wall. As time evolves, a counter-clockwise eddy is present at the intersection between the end wall and the line of separation. This eddy is intensified through flow entrainment and convects downstream with the primary flow. The critical point, classified as a node in the nomenclature of topological theory, becomes clearly visible at t = 400. The curved separation line in turn has an effect on the adjacent pair of lines of reattachment. The line of separation curves in the downstream direction. The distortion of downstream velocity is particularly pronounced near the singular node. In contrast, the line of reattachment curves towards the upstream side. The distortion is severe, in particular, in the span location where the separation line x_4 has its largest curvature near the location at $x = x_4$. As a result, the distance between the x_4 and x_5 lines reaches a minimum at the critical node. This distance continues to decrease with time; finally, at time $t > 700$, the roof eddy is only visible on the roof in the immediate vicinity of the end wall. This plot corresponds to Fig. 4, which shows that x_4 and x_5 cease to appear on the midplane at t = 700.

On the channel floor, we can clearly see the line of reattachment for the primary separation bubble from the computed limiting streamlines shown in Fig. 6. Revealed by this figure is a slight overshoot in the separation line x_1 at time $t \sim 400$. At the intersection of the step plane and the channel floor, one can observe overshoots. This critical point is by definition a separation saddle, from which streamlines repeal. This wall-oriented critical point moves towards the midplane as time increases. When $t > 700$, this critical point no longer varies in the y direction.

5. Conclusion

In this paper, we have focused on a three-dimensional flow in a channel with sudden expansion since there have been relatively very few computational studies. Results show that there is generally good agreement between the three-dimensional results and the experimental data for $Re <$ 400. Also, the agreement of three- and two-dimensional computed results is rather promising. The results reveal that as the Reynolds number increases, longitudinal vortices can evolve to the extent that the two-dimensional character of the flow is largely destroyed. Immediately away from the end wall, the x_1-curve on the midplane has a marked variation with the coordinate y. As to the secondary separation bubble on the roof of the channel, it is only visible near the end wall. We have also plotted the secondary flow patterns to provide evidence of the complex interaction of the end-wall-induced spiraling vortices with the flow through the three-dimensional channel expansion. This transient analysis has revealed the time-evolving penetration of the three-dimensional flow structure into a region of essentially two-dimensional flow near the midplane of the channel.

References

1. B. F. Armaly, F. Durst, J. C. F. Pereira, B. Schonung, "Experimental and theoretical investigation of backward-facing flow", J. Fluid Mech.

127, 473-496 (1983).

2. B. Jiang, L. Hou, and T. Lin, "Least-squares finite element solutions for three-dimensional backward-facing step flow", NASA-TM 106353 (1993).
3. P. T. Williams, A. J. Baker, "Incompressible computational fluid dynamics and the continuity constraint method for the three-dimensional Navier-Stokes equations", Numerical Heat Transfer, Part B, 29, 137-273 (1996).
4. P. T. Williams, A. J. Baker, "Numerical simulations of laminar flow over a 3D backward-facing step", Int. J. Numer. Meth. Fluids, 24, 1159-1183 (1997).
5. T. P. Chiang, Tony W. H. Sheu, S. F. Tsai, "Topology flow structure in backward-facing step channel", Computer and Fluids, 26, No. 4, 321-337 (1997).
6. T. P. Chiang, Tony W. H. Sheu, "Vortical flow over a 3D backward-facing step", Numerical Heat Transfer, Part A, 31, 167-192 (1997).
7. B. P. Leonard, "A stable and accurate convective modeling procedure based on quadratic upstream interpolation", Comput. Methods Appl. Mech. Engrg., 19, 59-98 (1979).
8. Van Doormaal J. P., and Raithby, G. D., 1984, "Enhancements of the SIMPLE method for predicting incompressible fluid flows," *Numerical Heat Transfer*, Vol. 7, pp.147-163.

Table 1. Grid and time sizes employed in the present study.

Grid-	N-*dx*	N-*dy*	N-*dz*	*dx*(*min, max*)	*dy*(*min, max*)	*dz*(*min, max*)
C	100	85	40	(0.03, 1.0)	(0.03, 0.25)	(0.03, 0.06)
D	90	25	22	(0.10, 0.6)	(0.03, 2.00)	(0.03, 0.16)

The time step dt = 0.02, 0.05, 0.1, 0.2, 0.5, 1.0, and 2.0 for the transient time, t, range in the interval: [0.0, 0.1], [0.1, 1.0], [1.0, 2.0], [2.0, 4.0], [4.0, 10.0], [10.0, 300.0], [300.0, 2000.0].

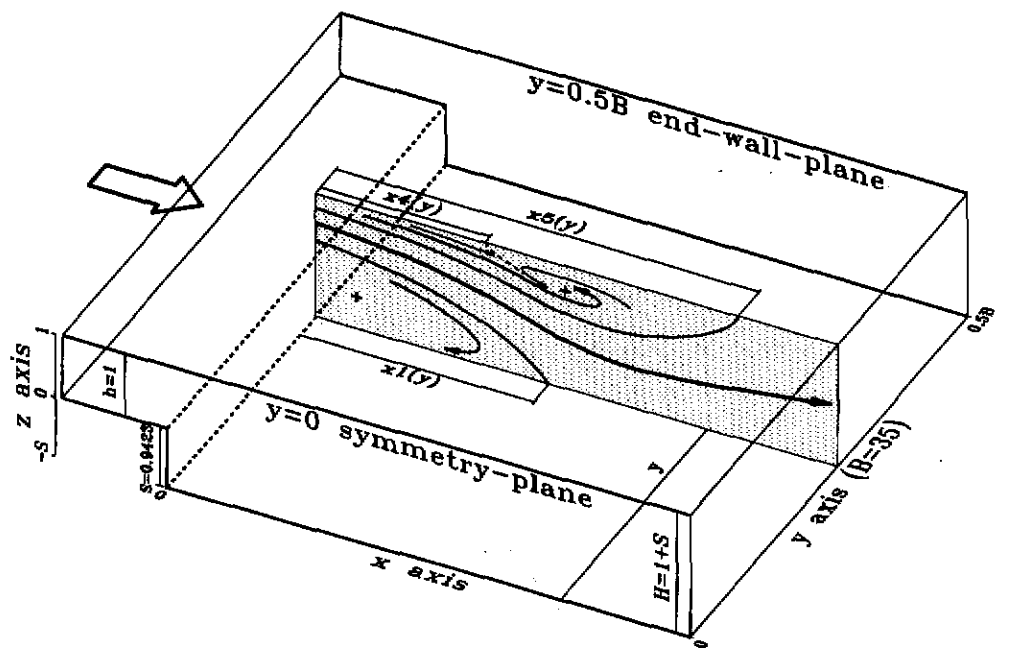

Fig. 1 Geometry of the backward-facing step channel flow under investigation.

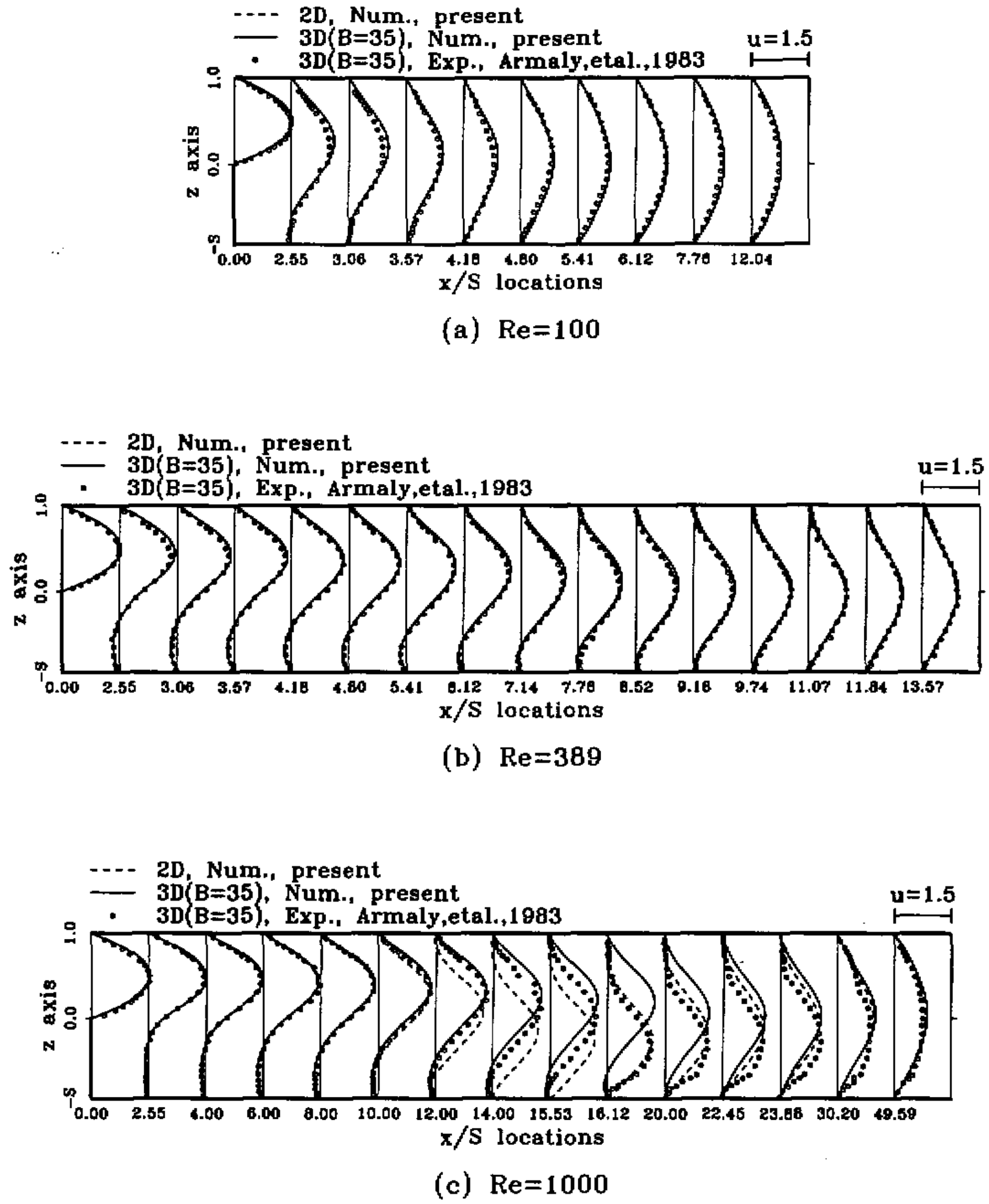

Fig. 2 Computed streamwise velocity profiles on the symmetry-plane of the channel. (a) $Re = 100$; (b) $Re = 389$; (c) $Re = 1000$.

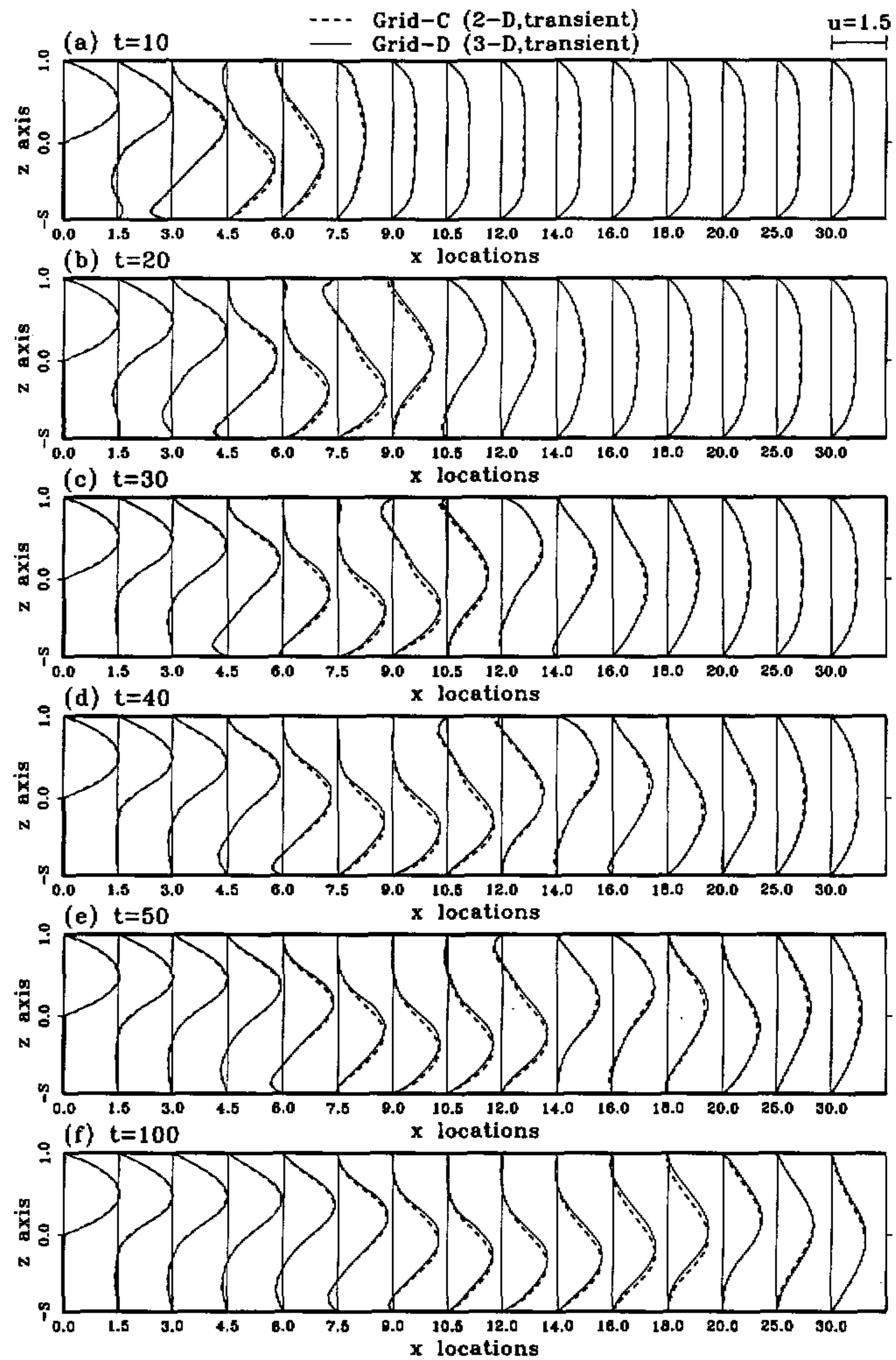

---- Grid-C (2-D,transient)
—— Grid-D (3-D,transient)
u=1.5
(a) t=10
(b) t=20
(c) t=30
(d) t=40
(e) t=50
(f) t=100
z axis
1.0
0.0
-5
0.0 1.5 3.0 4.5 6.0 7.5 9.0 10.5 12.0 14.0 16.0 18.0 20.0 25.0 30.0
x locations

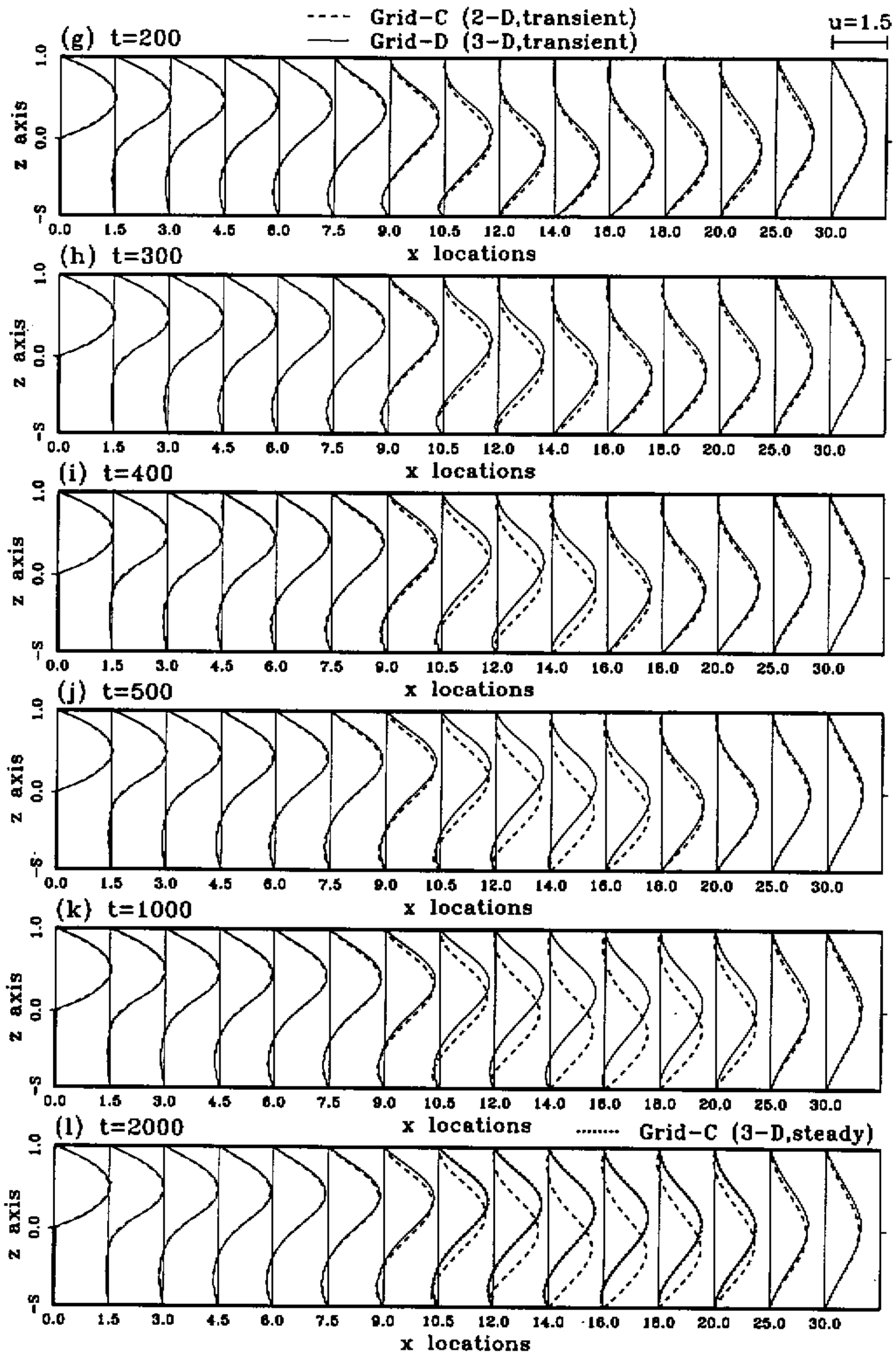

Fig. 3 Time history of streamwise velocity profiles on the symmetry-plane for the case of Re = 1000. (a) t = 10; (b) t = 20; (c) t = 30; (d) t = 40; (e) t = 50; (f) t = 100; (g) t = 200; (h) t = 300; (i) t = 400; (j) t = 500; (k) t = 1000; (l) t = 2000.

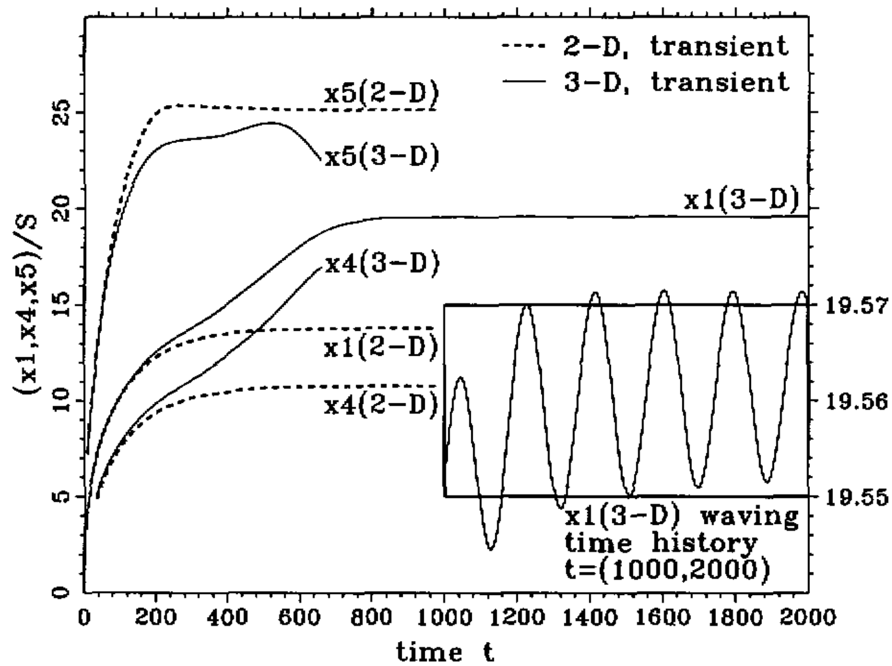

Fig. 4 Time history of x_1, x_4, and x_5 lengths, computed at the symmetry-plane of the channel, for the case of $Re = 1000$.

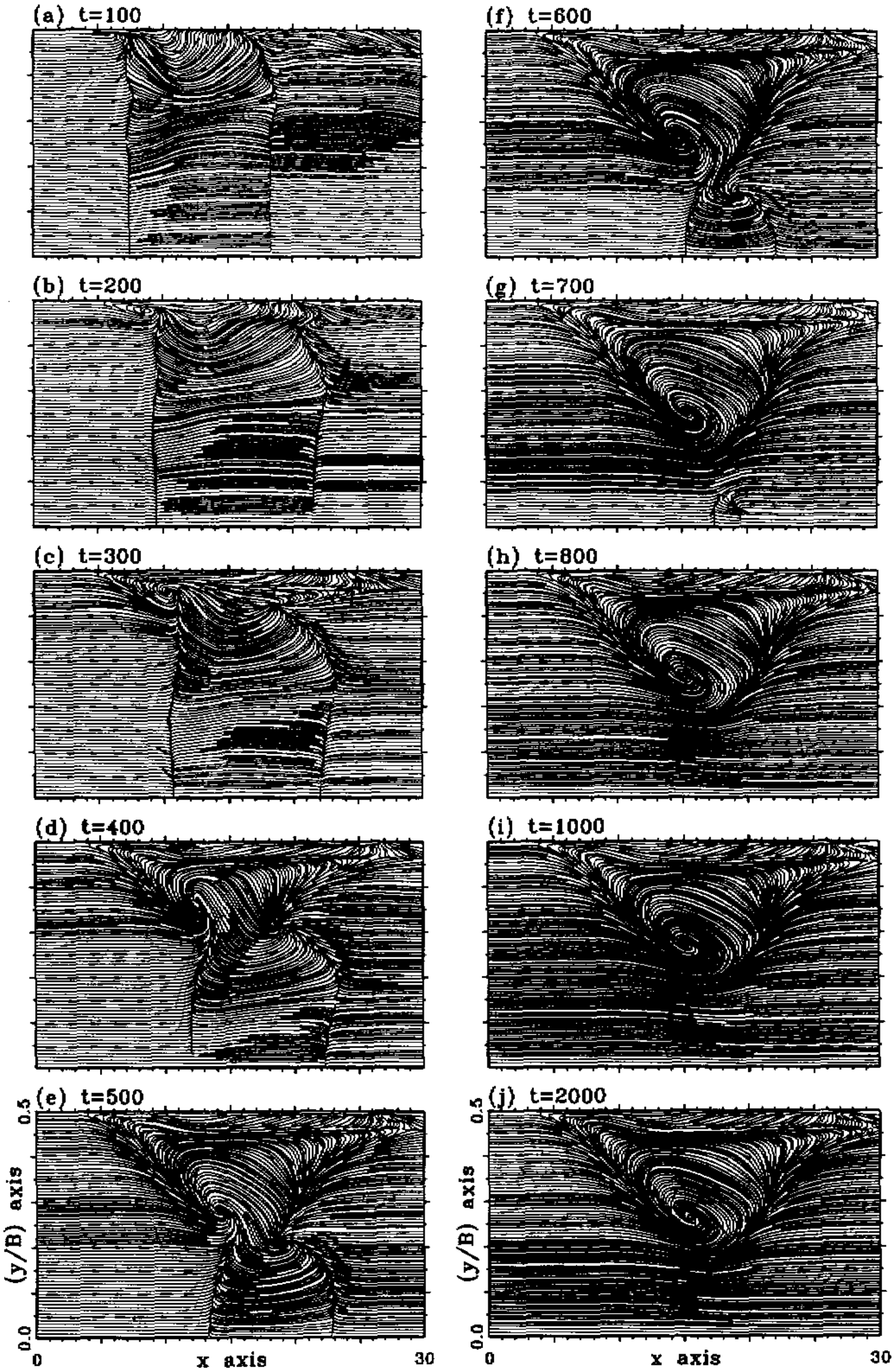

Fig. 5 Time history of limiting streamlines plotted on the roof of the channel for the case with $Re = 1000$. (a) $t = 100$; (b) $t = 200$; (c) $t = 300$; (d) $t = 400$; (e) $t = 500$; (f) $t = 600$; (g) $t = 700$; (h) $t = 800$; (i) $t = 1000$; (j) $t = 2000$.

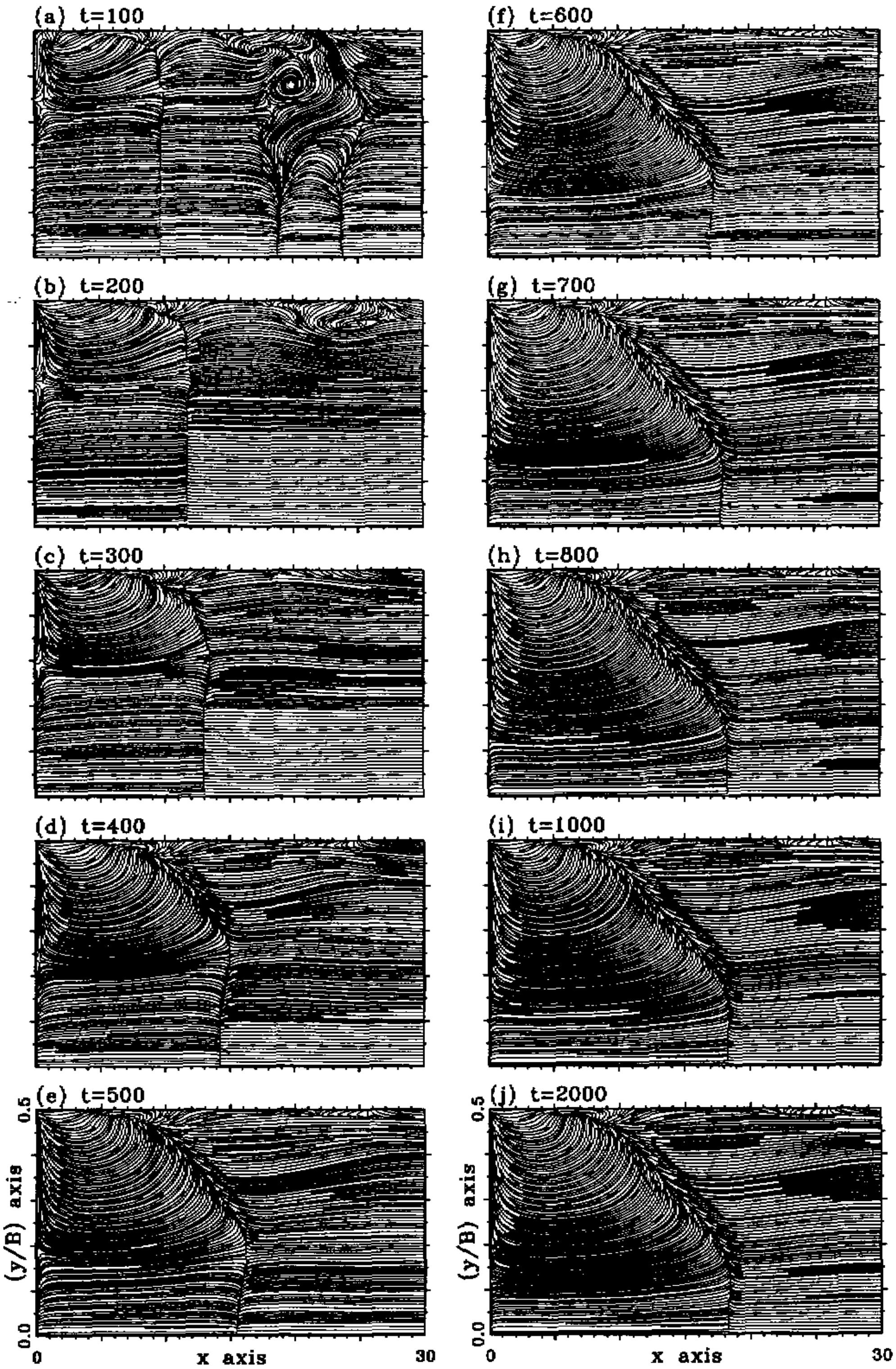

Fig. 6 Time history of limiting streamlines plotted on the floor of the channel for the case with $Re = 1000$. (a) $t = 100$; (b) $t = 200$; (c) $t = 300$; (d) $t = 400$; (e) $t = 500$; (f) $t = 600$; (g) $t = 700$; (h) $t = 800$; (i) $t = 1000$; (j) $t = 2000$.